Sensors & Actuators: A. Physical 396 (2025) 117213

Contents lists available at ScienceDirect

Sensors and Actuators: A. Physical

journal homepage: www.journals.elsevier.com/sensors-and-actuators-a-physical

A multi-wavelength, rigid-flex wearable ring oximeter for mitigating motion and skin pigmentation challenges: Hardware development and preliminary characterization ☆

Pilar Martín-Escudero [a],*, Ana M. Cabanas [b]

[a] Medical School of Sport Medicine, Faculty of Medicine, Universidad Complutense de Madrid, Madrid 28040, Spain
[b] Departamento de Física, Universidad de Tarapacá, Arica 1010069, Chile

ARTICLE INFO

Keywords:
Pulse oximeter
Wearable sensors
Point-of-care testing (POCT)
Photoplethysmography
Motion artifacts
Health equity

ABSTRACT

Pulse oximetry faces well-documented accuracy challenges related to skin pigmentation and motion artifacts, contributing to significant health disparities. In response, we present a wearable ring-type pulse oximeter designed to address these limitations through multi-wavelength sensing and stable anatomical coupling. The device features a rigid-flex printed circuit board integrating four LEDs (610–940 nm), dual photodetectors in transmission configuration, and a three-axis accelerometer. A Bluetooth-enabled microcontroller with adaptive acquisition firmware manages the system. The prototype was successfully fabricated and functionally validated. Optoelectronic characterization confirmed wavelength-dependent signal properties, with superior performance at longer wavelengths (740–940 nm). Preliminary testing on four healthy volunteers (Fitzpatrick skin types I–III) demonstrated reliable photoplethysmographic signal acquisition with improved signal-to-noise ratios at longer wavelengths, validating the hardware architecture's capability to acquire high-quality multi-wavelength PPG signals. This platform establishes technical feasibility for future clinical validation. However, validation against arterial blood gas analysis across all Fitzpatrick types (I–VI), systematic motion artifact assessment, and melanin-compensated SpO_2 algorithm development remain essential before clinical deployment.

1. Introduction

Pulse oximetry, once considered a mature and reliable technology, is now facing pivotal reevaluation driven by mounting clinical evidence of critical performance deficiencies. Data highlighting systematic measurement bias, particularly in individuals with darker skin tones, has prompted regulatory agencies including the U.S. Food and Drug Administration (FDA) and European authorities to issue safety communications and revised guidelines [1–3]. Recent meta-analyses encompassing thousands of patients have confirmed statistically significant overestimation of oxygen saturation in darker-pigmented individuals, with bias exceeding 1% in many commercial devices, sufficient to increase occult hypoxemia rates from 2% to 12% at clinically relevant SpO_2 thresholds [4–6]. This convergence of clinical evidence, regulatory action, and technological limitations has revealed a pressing gap in care equity, underscoring the urgent need for next-generation oximeters designed with robustness and inclusivity at their core [7,8].

The disparity in pulse oximeter accuracy stems from fundamental technical challenges in photoplethysmographic (PPG) signal acquisition. Skin pigmentation bias occurs when epidermal melanin, which strongly absorbs light at shorter wavelengths, alters the pulsatile AC/DC ratio used in conventional two-wavelength SpO_2 calculations [9–11]. Monte Carlo modeling has demonstrated that surface reflection and epidermal coupling amplify these spectral effects, particularly in reflectance-mode sensors [12]. Compounding this are motion artifacts, which introduce non-physiological signals overlapping in frequency with cardiac pulsations (0.5–5 Hz), making them difficult to remove through conventional filtering [13–15]. These technical limitations are particularly problematic in wearable applications, where users experience varied skin tones, activity levels, and environmental conditions that stress conventional calibration approaches developed primarily using light-skinned, resting participants [2,16].

Current approaches to address these limitations include multi-wavelength sensing strategies incorporating longer near-infrared wavelengths less affected by melanin, objective skin-tone quantification using Individual Typology Angle (ITA) or melanin index measurements for personalized calibration, and advanced signal processing algorithms combining motion sensors with machine learning for artifact

☆ This article is part of a Special issue entitled: 'In-Memory Sensing and Computing' published in Sensors and Actuators: A. Physical.

* Corresponding author.
E-mail addresses: pmartinescudero@med.ucm.es (P. Martín-Escudero), acabanas@academicos.uta.cl (A.M. Cabanas).

https://doi.org/10.1016/j.sna.2025.117213
Received 20 July 2025; Received in revised form 14 October 2025; Accepted 27 October 2025
Available online 4 November 2025

removal [10,17–19]. Recent validation studies have demonstrated that ring-form oximeters utilizing palmar measurement sites can achieve negligible bias across diverse skin tones under controlled hypoxic conditions, while tactile-intelligence approaches have shown up to 8-fold reduction in motion-related measurement error [19,20]. However, these solutions remain largely in research phases, and the rapid expansion of the wearable oximetry market, projected to exceed US$6 billion by 2034, demands practical, validated approaches implementable in consumer devices while meeting evolving regulatory standards [21,22].

To address these challenges, we present the development and preliminary characterization of a multi-wavelength, rigid-flex wearable ring oximeter designed to provide the technical foundation for improved measurement accuracy across diverse skin tones and during motion. The device integrates four LEDs spanning 610–940 nm with dual photodetectors in transmission configuration, enabling future algorithms to differentiate melanin absorption from hemoglobin dynamics. Built on a rigid-flex PCB platform with Bluetooth connectivity and adaptive firmware, the system demonstrates feasibility of continuous multi-wavelength PPG acquisition in a wearable form factor. This work focuses on hardware development and preliminary functional characterization, establishing the technical groundwork for future clinical validation studies across diverse populations.

This work demonstrates the technical feasibility of a multi-wavelength anatomically stable sensing platform as foundation for future validation studies aimed at improving oximetry equity and robustness. Clinical validation against gold-standard arterial blood gas analysis, systematic evaluation across diverse skin tones (Fitzpatrick types I–VI), and quantitative assessment of motion artifact compensation have not been performed and represent essential next steps before any claims of improved accuracy or equity can be substantiated.

2. Materials and methods

2.1. System architecture and design rationale

This study introduces a wearable pulse oximeter designed to address two major limitations in current technologies: motion artifact sensitivity and reduced accuracy in individuals with darker skin pigmentation [2,23,24]. The ring-shaped form factor enhances comfort, enables long-term use, and improves signal consistency. Compared to fingertip clips or wristbands, the ring provides stable skin contact, essential for reliable photoplethysmography (PPG) during movement or sleep [25].

A rigid-flex Printed Circuit Board (PCB) integrates all electronics into a compact structure conforming to the finger. This combination of rigid sections for mounting sensitive components and flexible interconnects enables natural wrapping around the finger, resulting in a lightweight, robust design with fewer connectors and reduced mechanical failure risk.

As shown in Figs. 1 and 2, the system consists of three interconnected PCBs: a central processor (TEK077), an emitter (TEK078), and a detector (TEK079), configured for transmission-mode pulse oximetry where light emitted from one side of the finger is captured on the opposite side after passing through tissue.

The central processing board (TEK077) houses a Nordic nRF52833 microcontroller handling system operations, signal processing, and Bluetooth communication, plus an ADPD4100 analog front-end (Analog Devices) synchronizing LED pulses with photodiode readings. The emitter board (TEK078) includes four LEDs at 610, 740, 850, and 940 nm, broader spectral coverage than conventional red/IR systems, supporting future algorithms for separating hemoglobin and melanin absorption to minimize skin-tone bias. The detector board (TEK079) houses two BPW34S photodiodes (430–1100 nm sensitivity) ensuring efficient transmitted light capture.

2.2. Optomechanical integration and anatomical targeting

The rigid-flex design enables careful spatial alignment of the emitter and detector boards around the finger, as shown in Fig. 2. The processor lies dorsally, with the optoelectronic units positioned laterally for a transverse optical path.

A key design objective was to target the digital arteries, where pulsatile signals are strongest. As illustrated in Fig. 3, the system's geometry was optimized based on vascular anatomy to minimize interference from non-pulsatile structures like bone and tendon. To account for anatomical differences, emission angles of 20° and 30° were tested, and the emitter-detector distance can be adjusted. This modular approach supports future optimization under varied conditions, including motion, darker skin pigmentation, and low perfusion states.

2.3. Component selection and system specifications

Component selection was guided by the need for a reliable, multi-wavelength oximetry platform capable of operating accurately under motion and across diverse skin tones. Rather than optimizing individual components in isolation, choices were made to support a cohesive system architecture that enables advanced signal processing and future algorithmic development.

The core innovation lies in the four-wavelength optical design (610, 740, 850, 940 nm), strategically selected to address limitations of conventional two-wavelength systems. Light transmission through tissue follows the modified Beer–Lambert Law:

$$I(\lambda) = I_0(\lambda) \cdot \exp\left[-\mu_a(\lambda) \cdot L\right] \tag{1}$$

where total absorption is $\mu_a(\lambda) = \sum_i \varepsilon_i(\lambda) \cdot C_i$, with ε_i as molar extinction coefficients and C_i as chromophore concentrations [26].

Conventional two-wavelength (660/940 nm) systems assume negligible melanin contribution:

$$\mu_a(660) \approx \varepsilon_{\mathrm{HbO_2}}(660) \cdot [\mathrm{HbO_2}] + \varepsilon_{\mathrm{Hb}}(660) \cdot [\mathrm{Hb}] \tag{2}$$

This assumption fails in individuals with elevated melanin, causing systematic overestimation of SpO_2 [10,27,28]. Four wavelengths enable explicit melanin estimation through an overdetermined system:

$$\begin{bmatrix} \mu_a(610) \\ \mu_a(740) \\ \mu_a(850) \\ \mu_a(940) \end{bmatrix} = \begin{bmatrix} \varepsilon_{\mathrm{HbO_2}}(610) & \varepsilon_{\mathrm{Hb}}(610) & \varepsilon_{\mathrm{mel}}(610) \\ \varepsilon_{\mathrm{HbO_2}}(740) & \varepsilon_{\mathrm{Hb}}(740) & \varepsilon_{\mathrm{mel}}(740) \\ \varepsilon_{\mathrm{HbO_2}}(850) & \varepsilon_{\mathrm{Hb}}(850) & \varepsilon_{\mathrm{mel}}(850) \\ \varepsilon_{\mathrm{HbO_2}}(940) & \varepsilon_{\mathrm{Hb}}(940) & \varepsilon_{\mathrm{mel}}(940) \end{bmatrix} \times \begin{bmatrix} [\mathrm{HbO_2}] \\ [\mathrm{Hb}] \\ [\mathrm{Mel}] \end{bmatrix} \tag{3}$$

This formulation enables melanin-corrected SpO_2 calculation: $SpO_2 = \frac{[\mathrm{HbO_2}]}{[\mathrm{HbO_2}]+[\mathrm{Hb}]} \times 100\%$ [28]. The wavelength selection follows established principles [29,30]:

610 nm (Amber): Functions as a melanin probe with high sensitivity ($\varepsilon_{\mathrm{mel}}(610) \approx 1.7 \times 10^6\ \mathrm{cm^{-1}M^{-1}}$), capturing superficial interactions where pigmentation dominates [31].

740 nm (Near-Infrared 1): Strategically positioned between conventional wavelengths, offering 60% reduced melanin interference versus 660 nm while maintaining differential HbO_2/Hb absorption. Penetration depth increases 30%–40%, ensuring adequate arterial signal in moderately pigmented tissue.

850 nm (Near-Infrared 2): Provides 75% lower melanin interference than 660 nm with excellent deoxygenation sensitivity. Reduced scattering coefficient ($\mu_s'(850) \approx 0.6 \times \mu_s'(660)$) improves motion stability.

940 nm (Near-Infrared 3): Reference channel with minimal melanin interference and maximum penetration, near the hemoglobin isosbestic point for stable total hemoglobin measurement.

Melanin absorption decreases as $\lambda^{-3.46}$ [26]. The wavelength-dependent optical penetration depth (δ) in tissue follows:

$$\delta(\lambda) \approx \frac{1}{\sqrt{3\mu_a(\lambda)\mu_s'(\lambda)}} \tag{4}$$

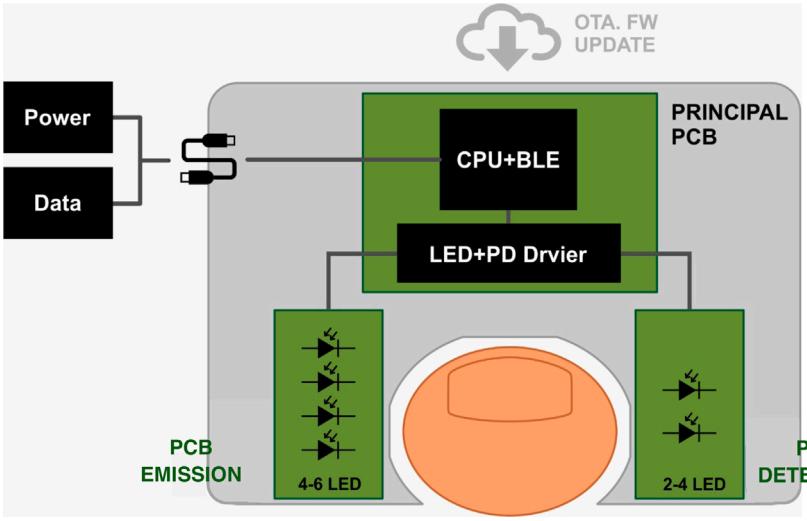

Fig. 1. System architecture of the ring oximeter showing processing, power, and optoelectronic subsystems.

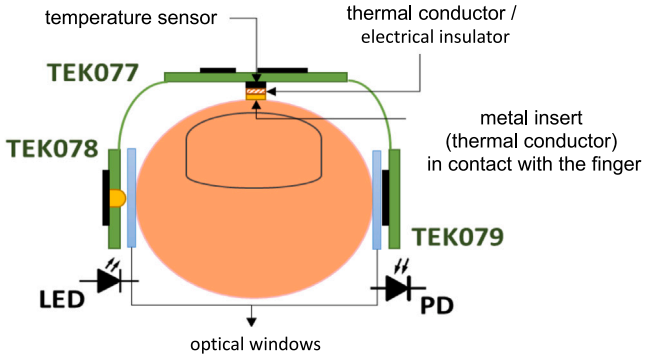

Fig. 2. Anatomical adaptation of the ring oximeter, with opposing LEDs and photodetectors.

In lightly pigmented skin (Fitzpatrick types I–III): $\delta(660) \approx 2$–3 mm, $\delta(940) \approx 4$–6 mm. In highly pigmented skin (Fitzpatrick types V–VI): $\delta(660) \approx 1$–1.5 mm, $\delta(940) \approx 3$–4 mm. The inclusion of intermediate wavelengths (740, 850 nm) with moderate penetration depths ensures that at least one channel achieves adequate arterial signal quality even when the 610 nm channel is severely attenuated by superficial melanin.

The original 609 nm LED was replaced by Bivar SM1206NAC-IL (610 nm) after preliminary testing showed superior signal amplitude and sensitivity.

Table 1 summarizes the final configuration. High-sensitivity OSRAM BPW34S photodiodes (600–1000 nm, 0.62 A/W @ 940 nm) capture all wavelengths with minimal loss. The Analog Devices ADPD4100 analog front-end coordinates precise LED timing and synchronized acquisition with 8-channel capability, integrated current sources (200 mA max per channel), and low-noise amplification.

The Nordic nRF52833 microcontroller balances processing capability with power efficiency. Key specifications: BLE 5.0 connectivity, integrated voltage regulation, power consumption of 5–6 mA during radio operation and 1.8 μA in sleep mode with RAM retention, enabling extended battery operation in future implementations.

Thermal management utilizes a Panasonic PGS graphite sheet [32] for passive heat dissipation, maintaining wavelength stability during extended operation. Temperature monitoring with NTC thermistor (10 kΩ @25 °C) and automatic thermal shutdown ensures component protection and user safety.

Table 2 details additional capabilities. Over-the-Air (OTA) firmware updates enable iterative algorithm deployment without hardware modifications, essential for ongoing clinical validation.

The current prototype operates via USB for development and characterization. Future iterations will integrate battery management, optimize power consumption, and include accelerometer and ambient light sensors for enhanced motion artifact detection.

While this hardware platform provides capability for melanin-corrected algorithms through its four-wavelength design, the development and clinical validation of such algorithms requires extensive data collection across diverse populations. The theoretical advantages, including explicit melanin estimation and improved robustness to skin pigmentation, remain to be experimentally validated through rigorous clinical studies as outlined in the study limitations.

The complete system architecture supports advanced pulse oximetry research while maintaining flexibility for iterative development based on ongoing validation [7,33]. The design is protected under National Utility Model U202431452 [34–36].

2.4. Mechanical design and hardware integration

The mechanical design ensures reliable physiological signal acquisition through three priorities: long-term comfort, structural stability during motion, and precise optoelectronic alignment.

The device features a three-board rigid-flex PCB integrating the microcontroller, analog front-end, and optical sensors into a single assembly. This architecture, detailed in *Supplementary Material (Figures S1 and S2)*, was selected over traditional wired connections to improve durability, simplify assembly, and enable compact anatomical conformity. As shown in Fig. 4 (right panel), flexible polyimide interconnects allow the emitter and detector boards to bend at 90°, forming a stable transmission-mode setup across the digit.

A custom enclosure was developed through iterative 3D printing for rapid prototyping and ergonomic evaluation. It consists of a central body (TEK077) housing the processing unit, and two lateral arms for the emitter (TEK078) and detector (TEK079). This configuration ensures stable sensor-skin contact, minimizing motion artifacts in PPG signals.

The internal frame (Fig. 4, middle panel) maintains precise PCB alignment during activity. To accommodate anatomical variability, three adjustable-height versions enable ±1.5 mm vertical positioning of emitter and detector to optimize artery alignment and avoid bone/tendon interference.

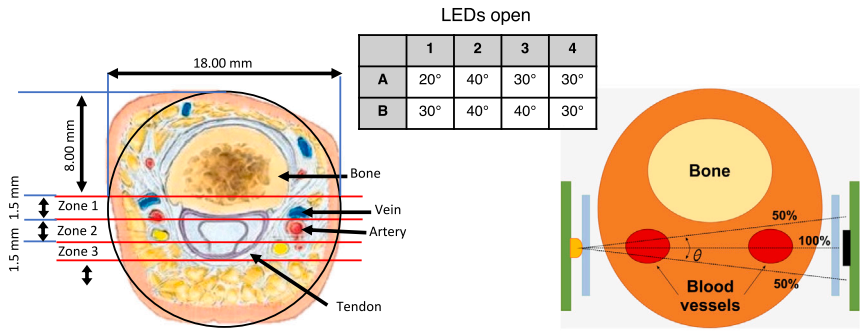

	1	2	3	4
A	20°	40°	30°	30°
B	30°	40°	40°	30°

Fig. 3. LED emission angles (20° and 30°) and detector placement for optimal vascular targeting.

Table 1
Final hardware specifications and selected components.

Component category	Selected components and specifications
LED emitters (4 active)	Bivar SM1206NAC-IL (610 nm, optimized selection) OSA Opto Light OIS-330 740 (740 nm) Wurth Elektronik 15412085A3060 (850 nm) Harvatek B15V1IR-A1C00015 (940 nm)
Photodetectors	2 × OSRAM BPW34S (600–1000 nm, 0.62 A/W @ 940 nm)
LED/PD driver	Analog Devices ADPD4100 (8 LEDs, 8 PDs, 200 mA max per channel)
Main controller	Laird BL653μ (Nordic nRF52833), BLE 5.0, 512 kB Flash, 128 kB RAM
Power management	Integrated LDO/DC-DC, 1.7–5.5 V supply, 1.8 μA sleep current
Thermal management	Panasonic PGS graphite sheet (25 μm, 1700 W/m K) + Cu thermal bridge

Table 2
Advanced system features and specifications.

Feature	Specification/Implementation
Wireless connectivity	BLE 5.0, −20 to +8 dBm configurable output power
Firmware updates	OTA capability via BLE interface
Data storage	512 KB Flash, 128 KB RAM, persistent parameter storage
Temperature monitoring	NTC thermistor (10 kΩ @ 25 °C), thermal safety shutdown
Thermal management	Panasonic PGS graphite sheet + copper thermal bridge
Development interface	USB connection for programming, debugging, and power
Signal processing	Real-time PPG acquisition, heart rate estimation, adaptive timing

LED junction temperature directly impacts wavelength stability and device longevity. Peak wavelength typically shifts 0.2–0.5 nm/°C; a 5–10 °C increase causes 2–4 nm drift, potentially affecting SpO_2 accuracy given hemoglobin's narrow absorption spectrum [37–39].

The thermal management system employs a Panasonic PGS (Pyrolytic Graphite Sheet) between the LED substrate (TEK078) and a metallic bridge contacting the finger. PGS provides exceptional in-plane thermal conductivity (1500–1950 W/m K), approximately four times higher than copper, while remaining flexible at only 25 μm thickness [40].

The thermal path operates as follows: (1) heat transfers from LED junctions to PCB copper traces; (2) PGS spreads heat laterally, preventing hot spots; (3) a copper insert (Fig. 4B) conducts heat to the finger surface; (4) the finger acts as a heat sink at 32–34 °C under normal conditions. PGS key specifications: in-plane thermal conductivity 1500–1950 W/m K, through-plane conductivity 10 W/m K, thermal resistance 0.14–0.40 °C cm^2/W (thickness-dependent), operating range −40 °C to +400 °C, flexibility for radii <5 mm. With pulsed LED operation (duty cycle 1%, peak currents 65–110 mA), average power per LED is 15–25 mW. Thermal modeling estimates junction temperature rise of only 0.3–0.6 °C above skin temperature, yielding wavelength shift <0.2 nm, negligible relative to hemoglobin absorption bandwidth. Low duty cycle limits heat accumulation while PGS and thermal bridge ensure efficient dissipation.

A contact NTC thermistor (10 kΩ @ 25 °C) on TEK077 near the LED substrate enables real-time temperature monitoring. While not used for active correction in this prototype, it supports thermal safety limits (automatic LED shutdown above 45 °C). Future firmware may incorporate temperature-based wavelength calibration for enhanced stability.

The 850 nm and 940 nm LEDs operate in the near-infrared where ambient IR can introduce noise. Mitigation strategies include: (1) finite impulse response (FIR) digital filtering; (2) LED drive currents limited to component ratings (Table 3) or 200 mA per ADPD4100 channel; (3) transmission-mode geometry with protective optical windows providing partial shielding.

The complete assembly (Fig. 4, left panel) integrates all components into a compact, wearable form. The protective shell supports extended use and physical activity while maintaining emitter-detector alignment. Future iterations will use biocompatible medical-grade elastomers to meet regulatory standards for skin-contact devices.

This modular design ensures consistent signal quality across users with varying anatomy and under motion. By embedding optomechanical alignment in the rigid-flex architecture, the platform provides a robust foundation for high-fidelity physiological monitoring in real-world conditions.

2.5. Prototype fabrication and physical implementation

Following hardware and mechanical design completion, physical prototypes were fabricated to validate integration, functionality, and ergonomic performance, a critical step in demonstrating feasibility of the engineered solution.

The core electronic assemblies were built as Minimum Viable Prototypes (MVPs), based on a custom rigid-flex PCB architecture. This design integrates the central processing unit and lateral optoelectronic

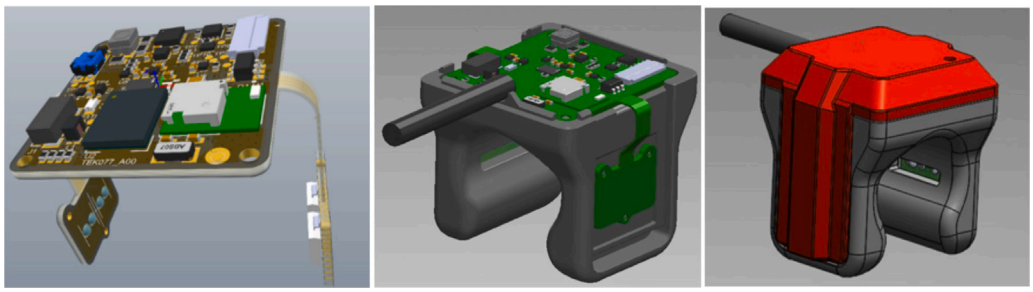

Fig. 4. Mechanical design and integration of the ring oximeter. (Right) Rigid-flex PCB with LEDs and photodiodes at 90° angles for transmission-mode alignment. (Middle) Internal enclosure showing PCB modules and embedded thermal bridge. (Left) Final assembly with protective shell, designed for prolonged wear and stable alignment.

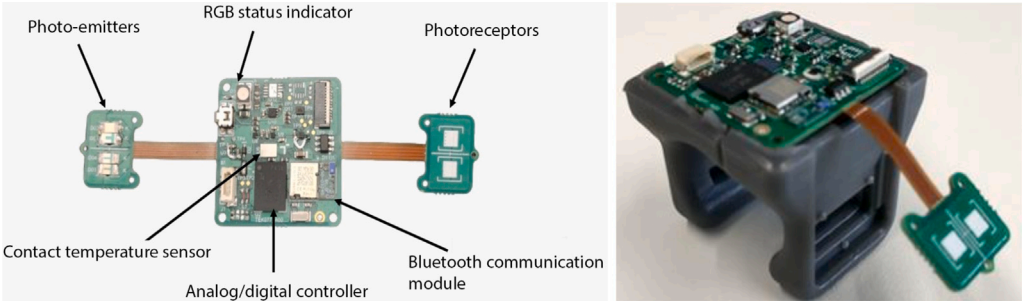

Fig. 5. Prototype fabrication and integration of the ring oximeter. (Right) Fabricated rigid-flex PCB with integrated optoelectronics. (Left) Final MVP assembly with 3D-printed enclosure, showing ergonomic form and maintained alignment.

modules into a single, connector-free assembly, eliminating common failure points and enabling a compact, conformal wearable structure.

To ensure ergonomic conformity and stable optoelectronic alignment, 3D-printed mechanical enclosures were fabricated with vertical adjustment capability for optical components, enabling proper vascular alignment across varying finger anatomies and maximizing signal quality in transmission-mode oximetry. The complete implementation is shown in Fig. 5. The right panel presents the fabricated rigid-flex PCB assembly with mounted emitters and detectors. The left panel shows the final integrated MVP within its mechanical enclosure, forming a compact wearable device with stable optoelectronic alignment.

Physical features validated during prototyping include: internal structural frame ensuring precise PCB positioning, flexible interconnects allowing angular adjustment of optoelectronic modules (Fig. 4), and enclosure accommodation of multiple optical path heights. These mechanical features were iteratively refined through ergonomic testing to ensure anatomical conformity, signal stability, and comfort during prolonged use.

The physical layout of the four-wavelength emitter board is detailed in Fig. 6. The wavelength selection (610, 740, 850, 940 nm) was strategically chosen to address limitations of conventional two-wavelength pulse oximeters. Shorter wavelengths (610 nm) exhibit higher sensitivity to superficial melanin, while longer wavelengths (740–940 nm) penetrate deeper with reduced melanin interference, enabling differential analysis of hemoglobin and melanin absorption, a critical requirement for equitable SpO_2 measurement across diverse skin tones.

The specific arrangement and firmware identifiers (LED_x) allow the ADPD4100 analog front-end and nRF52833 microcontroller to precisely sequence LED activation and synchronize photodiode acquisition, forming the multi-channel data foundation for advanced SpO_2 and motion correction algorithms.

This fabrication and assembly process validates the mechanical and electronic integration necessary for a functional wearable oximetry platform. The modular design supports iterative refinement based on preliminary testing and future clinical validation requirements.

2.6. Optoelectronic calibration protocol

Prior to functional testing, the device underwent systematic optoelectronic calibration to determine optimal LED operating parameters and validate photodetector response across the four wavelength channels. This preliminary characterization ensured each wavelength operated within design specifications and established baseline performance metrics for the multi-wavelength platform.

Calibration measurements were performed on four healthy volunteers (Fitzpatrick skin types I–III) under controlled laboratory conditions: ambient temperature 22 ± 2 °C, minimal ambient light to reduce optical interference. Participants were seated at rest with the device positioned on the index finger. No formal clinical protocol was employed, as the objective was hardware verification rather than clinical validation.

For each LED wavelength (640, 765, 860, 960 nm), drive current was systematically varied across four levels: 20, 65, 110, and 155 mA. These values span the operational range while remaining within safe component limits (Table 3). Photodetector output was recorded for 10 s at each current level, with 30-s rest intervals to prevent thermal accumulation and allow tissue temperature stabilization.

Raw photodetector data were analyzed to extract: (1) signal amplitude (peak-to-peak voltage of pulsatile AC component), and (2) baseline noise (standard deviation during diastolic periods). Signal-to-noise ratio (SNR) was calculated for each condition to quantitatively assess signal quality. Optimal drive currents were selected by maximizing SNR while remaining below 50% of maximum rated current, ensuring long-term reliability and minimizing thermal drift during extended monitoring.

Calibration results confirmed expected trends from optical tissue interaction theory [41]. Longer wavelengths (850–940 nm) exhibited higher signal quality at equivalent drive currents compared to shorter wavelengths. This wavelength-dependent performance is attributed to reduced scattering and melanin absorption in the near-infrared spectrum, permitting deeper photon penetration and stronger interaction with pulsatile arterial blood [31,42]. Conversely, the amber

Fig. 6. Physical layout and identifiers of the four LEDs. Wavelengths (610, 740, 850, 940 nm) were selected for differential tissue penetration and melanin sensitivity. Emission angles (Φ = 20–30°) optimize targeting of digital arteries for high-quality photoplethysmographic signals.

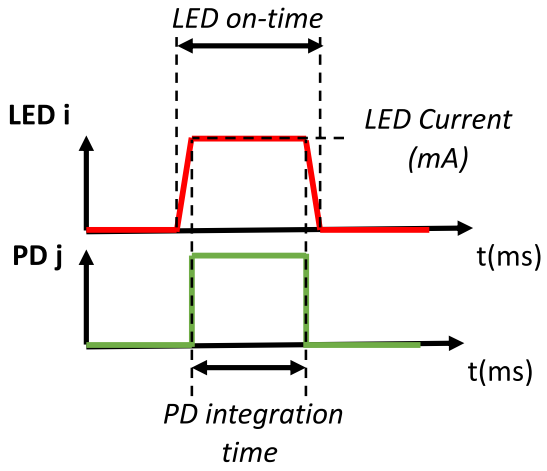

Fig. 7. Key configurable LED and PD timing parameters.

LED (640 nm) produced comparatively lower amplitude signals, consistent with increased superficial tissue scattering and higher melanin absorbance at shorter visible wavelengths.

During characterization, the original 609 nm LED showed insufficient signal amplitude. Following systematic evaluation, it was replaced with the Bivar SM1206NAC-IL (610 nm), which demonstrated superior emission efficiency and improved signal quality, justifying its selection for the final prototype configuration.

This calibration represents technical characterization of the optoelectronic subsystem, not clinical calibration against arterial blood gas measurements or co-oximetry. The procedure was limited to a small sample with light skin pigmentation (Fitzpatrick types I–III), and no hypoxic challenges or controlled desaturation protocols were implemented. These results validate hardware functionality and wavelength-dependent signal characteristics, but do not constitute evidence of clinical accuracy or equity across diverse populations.

A rigorous clinical calibration study is planned as the next development phase, including: (1) validation against arterial blood gas analysis (gold standard for SpO_2), (2) testing across the full Fitzpatrick scale (types I–VI), (3) controlled hypoxic chamber protocols assessing performance across oxygen saturation levels (70%–100%), and (4) compliance with updated FDA guidance for pulse oximeter evaluation in diverse populations [1]. Results will be reported in a subsequent publication.

2.7. Firmware architecture and adaptive measurement protocol

The firmware provides robust control over the optoelectronic system, wireless communication, and implements an intelligent, adaptive measurement protocol. Primary design goals: maximize signal quality, optimize power consumption for wearable applications, and establish a flexible framework for future advanced signal processing algorithms.

The firmware's measurement logic is built around configurable timing parameters illustrated in Fig. 7. These parameters, LED drive current, pulse duration, and photodiode (PD) integration time, enable precise optical front-end tuning. This configurability is essential for empirically optimizing signal-to-noise ratio (SNR) across different users and conditions. LED drive currents are managed within safe operational limits specified by component manufacturers (Table 3) and ADPD4100 driver capabilities, ensuring device longevity and user safety.

2.8. Adaptive dual-phase measurement workflow

To enhance measurement reliability, the firmware employs an adaptive, dual-phase workflow that alternates between heart rate (HR) estimation and multi-wavelength oximetry measurement. This "smart" cycle, depicted in Fig. 8, ensures that the acquisition of oximetry data is synchronized with the user's real-time cardiac cycle, a foundational strategy for improving resilience to motion artifacts and physiological variability.

The workflow begins with a 3-s HR estimation phase. During this window, only the 610 nm LED ($\mathbf{LED}_1$) is used to acquire a continuous PPG signal, sampled at approximately 100 Hz ($T_S \approx 10$ ms). The resulting high-resolution waveform is processed in real-time by an on-board peak detection algorithm to accurately determine the current heart rate.

Once a stable HR is established, the firmware transitions to the oximetry phase. In this stage, the system leverages the HR data to adaptively time the sequential pulsing of two LEDs per cardiac cycle: the 610 nm LED ($\mathbf{LED}_1$) and a second, configurable LED ($\mathbf{LED}_X$) from the remaining wavelengths. By synchronizing the LED pulses and corresponding photodiode integration windows (T_{PD}) with the detected heartbeat, the system can acquire high-resolution differential absorption data at the most information-rich points of the cardiac cycle. This phase lasts for approximately 10 s before the system reverts to the HR estimation phase to update the heart rate. An example of the raw PPG waveform captured during this dual-phase process is shown in Fig. 9.

All system parameters and data streaming are controlled via a command-line interface, which facilitates rapid prototyping and data analysis during development.

2.9. Signal processing and functional verification

Real-time heart rate (HR) estimation underpinning the adaptive measurement workflow employs a frequency-domain peak detection algorithm adapted from Argüello Prada [43]. This method was selected for computational efficiency, low complexity, and robust systolic peak identification in noisy photoplethysmographic (PPG) signals, ideal for power-constrained embedded systems.

The processing pipeline (Fig. 10) operates on 10-s filtered PPG segments. After applying Fast Fourier Transform (FFT) to generate the power spectrum, a robust peak detection algorithm identifies candidate cardiac frequencies within the physiological range (0.5–5 Hz, corresponding to 30–300 bpm). Harmonic analysis evaluates peak pairs and triplets using a heuristic scoring function favoring plausible cardiac

Table 3
Maximum allowable current levels for each LED. Calibration procedures for determining optimal operating currents are described in Section 2.6.

Range (nm)	Ref PCB	Reference	I_{op}	I_{max}	Conditions
600–670	D01	Wurth Elektronik 156120AS82500	20 mA	40 mA	$t_p \leq 1$ ms, duty $\leq 10\%$
740–800	D02	OSA Opto Light OIS-330 740	30 mA	150 mA	$t_p \leq 100$ µs, duty $\leq 10\%$
800–870	D03	Wurth Elektronik 15412085A3060	30 mA	150 mA	$t_p \leq 1$ ms, duty $\leq 5\%$
940–950	D04	Harvatek B15V1IR-A1C00015	100 mA	100 mA	$t_p \leq 1$ ms, duty $\leq 1\%$

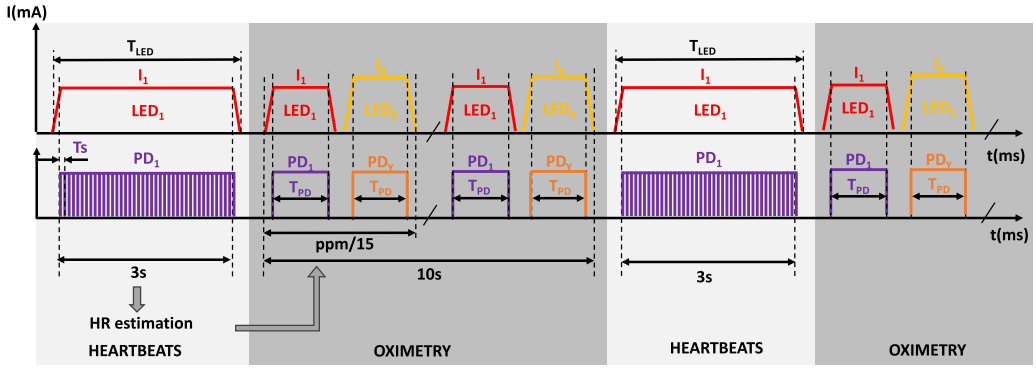

Fig. 8. Timing logic of the ring oximeter measurement cycle, showing the HR estimation window and the synchronized oximetry phase with LED and photodiode activation.

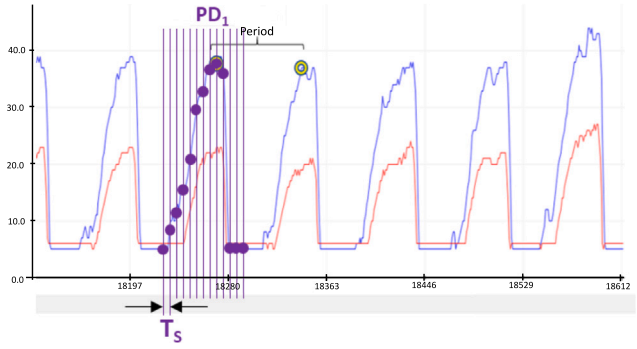

Fig. 9. Example of raw PPG waveform acquired during HR estimation and oximetry phases. The plot shows sampling intervals, photodiode integration windows, and LED pulse alignment.

harmonics while rejecting noise. The selected HR estimate is temporally smoothed using the previous value to ensure continuity and suppress transient artifacts.

Signal-to-noise ratio (SNR) is primarily determined by the pulse averaging configuration of the ADPD4100 front-end. Each PPG sample is calculated from the sum of n acquisition pulses. A single pulse yields SNR ≈ 76 dB, with maximum averaging increasing this to ≈100 dB. Doubling the number of pulses improves SNR by approximately 3 dB. When n is a multiple of 4, the ADPD4100 enables integrator chopping, alternating integration window polarity to cancel DC offset and low-frequency noise. The signal processing chain includes hardware anti-aliasing filters, Bessel band-pass filter (0.5–5 Hz), and moving average smoothing.

While the device hardware reliably acquires multi-wavelength PPG signals, a complete SpO_2 calculation algorithm has not yet been implemented. Developing an algorithm that separates melanin absorption from hemoglobin dynamics (Section 2.3) requires a dedicated calibration dataset including simultaneous PPG recordings and arterial blood gas reference measurements across diverse skin tones and oxygenation levels. This dataset will be collected during the clinical validation study described in Section 2.6. The current prototype demonstrates hardware and signal acquisition capability but does not compute SpO_2 values.

Preliminary functional testing confirmed the viability of both hardware and firmware. As shown in Fig. 11, PPG signals were acquired from four healthy volunteers (N = 4, Fitzpatrick skin types I–III) using all four LED channels. The figure displays representative data from one subject.

Visual inspection of the filtered signals reveals that longer wavelengths (740, 850, 940 nm) produce cleaner PPG waveforms with more distinct pulsatile components compared to the 610 nm LED. The 610 nm signal exhibits a higher noise floor relative to the cardiac pulsation amplitude, consistent with expected behavior: shorter wavelengths experience greater scattering and melanin absorption in superficial tissue layers, while longer wavelengths penetrate deeper with reduced interference [31,41].

Notably, the 610 nm LED operates at lower drive current (40 mA) compared to the other wavelengths (100 mA), partially accounting for the amplitude difference. However, even accounting for drive current differences, the wavelength-dependent signal quality trend aligns with optical tissue interaction principles. The 610 nm channel's sensitivity to superficial tissue properties makes it valuable for future melanin correction algorithms, while the near-infrared channels (740–940 nm) provide robust arterial pulsation signals suitable for oxygen saturation estimation.

These results validate that the multi-wavelength acquisition system successfully captures wavelength-dependent tissue optical properties, providing the spectral diversity required for future development of equitable SpO_2 estimation algorithms.

3. Discussion

The successful fabrication and testing of this prototype mark a foundational step in developing a next-generation physiological monitoring platform. This section analyzes verification results within the framework of light–tissue interaction physics and explores engineering implications for building more equitable and robust pulse oximetry systems.

3.1. Functional verification and optoelectronic performance

Initial testing validated multi-wavelength optoelectronic system performance. Results (Fig. 11) confirm hardware integrity and optical

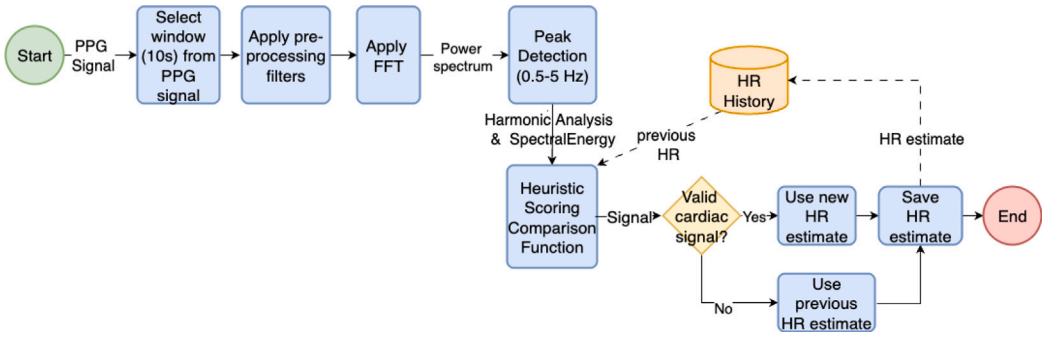

Fig. 10. Heart rate estimation algorithm flowchart. The pipeline processes 10-s PPG windows through FFT analysis, peak detection, harmonic evaluation, and temporal smoothing.

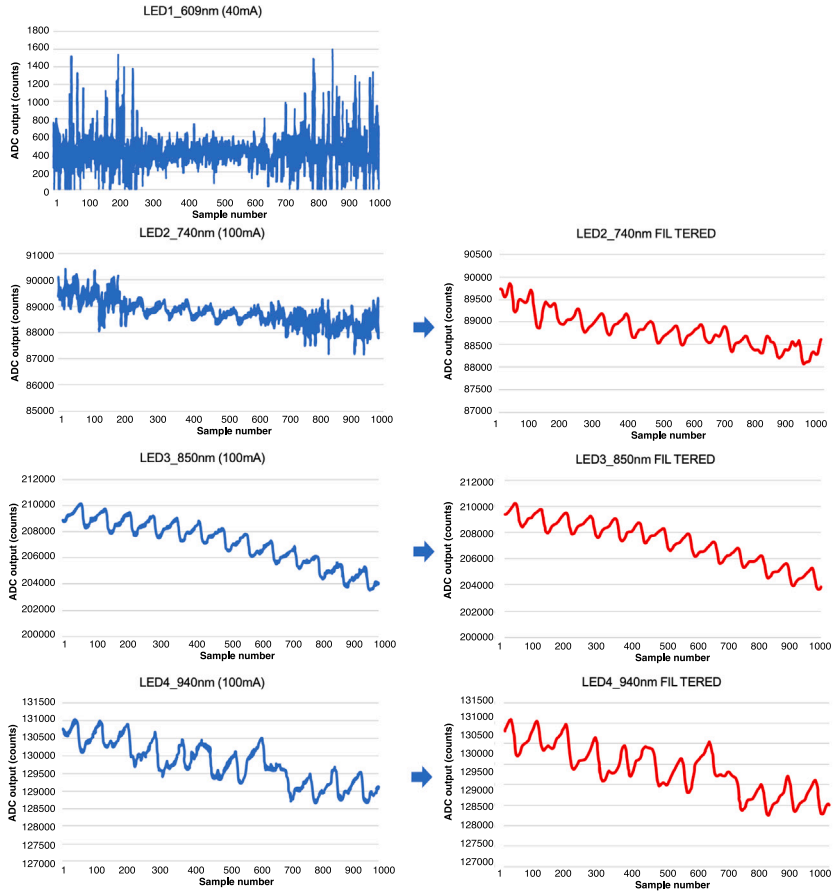

Fig. 11. Raw (left, blue) and filtered (right, red) PPG signals from four LEDs. The x-axis shows sample number; y-axis shows ADC output (counts) from the ADPD4100 front-end. Filtering used a Bessel bandpass filter (0.5–5 Hz). Higher signal-to-noise ratio is observed at longer wavelengths (740–940 nm) compared to 610 nm.

sensing viability in biological tissues. A clear trend emerged: as wavelength increased from 610 nm to near-infrared (740, 850, 940 nm), PPG signal-to-noise ratio improved significantly.

This observation confirms the wavelength-dependent performance predicted by optical tissue interaction physics (Section 2.3). Superior signal quality at longer wavelengths validates the multi-wavelength hardware platform design. Although the 610 nm LED produced relatively weak signals, this was expected. Its melanin sensitivity makes it valuable for identifying pigmentation-induced signal distortions, information essential for future algorithmic compensation. Its low amplitude is not a shortcoming but an informative asset critical for developing equitable measurement strategies.

3.2. Iterative sensor optimization and final wavelength configuration

During preliminary characterization, the original 610 nm LED exhibited low signal amplitude, limiting system sensitivity. An optimization procedure evaluated an alternative component: the Bivar SM1206NAC-IL (610 nm), offering similar wavelength but higher emission efficiency and improved operational stability.

Both LEDs were tested under identical conditions (same drive current, photodetector integration time, optical geometry) enabling direct performance comparison. Fig. 12 shows comparative signal traces. The Bivar SM1206NAC-IL demonstrated significantly higher signal amplitude, resolving the sensitivity limitation. Based on this experimental comparison, the Bivar component was selected for the final prototype.

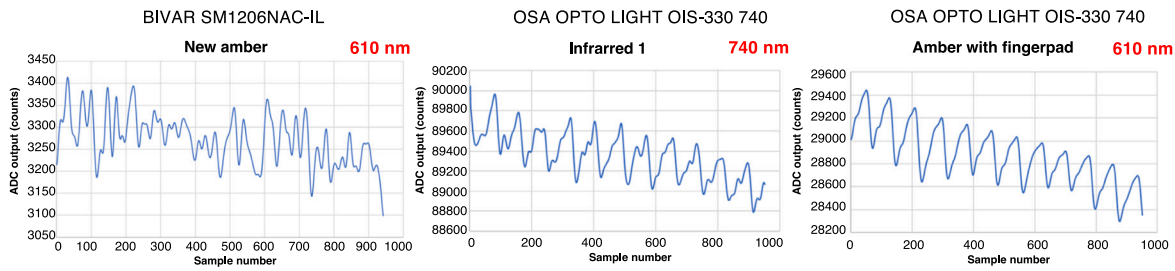

Fig. 12. Signal comparison for LED optimization. The x-axis shows sample number; y-axis shows ADC output (counts). Left: Bivar SM1206NAC-IL LED (610 nm); center: infrared LED (740 nm); right: original amber LED. The new amber LED demonstrates significantly improved signal amplitude, justifying its selection for the final prototype.

The final LED configuration (610, 740, 850, 940 nm) is detailed in Fig. 6 (Section 2). This multi-wavelength selection yields a multi-spectral dataset necessary to overcome limitations of traditional two-wavelength oximeters relying on one-size-fits-all calibration curves that fail to account for physiological differences such as skin pigmentation. The expanded spectral range enables the system to capture wavelength-dependent absorption differences between hemoglobin and melanin, laying the foundation for more equitable SpO_2 estimation algorithms.

3.3. Implications for future development

This study establishes proof-of-concept for an engineered sensing platform. Its key contribution lies not in delivering a finished clinical product, but in validating a hardware architecture capable of collecting multi-channel data required for advanced algorithm development. The embedded command-line interface proved essential for real-time system parameter tuning during characterization and optimization.

The next phase will focus on clinical validation and algorithmic innovation. With four spectral channels available, melanin contribution to overall absorption may be treated as a solvable variable rather than a confounding factor, allowing for more individualized, potentially calibration-free models. Such approaches could mark major advances in both accuracy and measurement equity.

3.4. Study limitations and future validation

This work demonstrates successful engineering and preliminary characterization of a multi-wavelength pulse oximeter platform. However, several important limitations must be acknowledged.

The device has not been validated against arterial blood gas analysis, the gold standard for oxygen saturation measurement. All tests were conducted under normoxic conditions ($SpO_2 > 95\%$) without controlled desaturation protocols; therefore, accuracy across the full physiological range (70%–100%) is unknown. This places the work at Technology Readiness Level (TRL) 2 to early TRL 3. While hardware feasibility and signal acquisition were achieved, key intended functions, motion artifact compensation and melanin-independent SpO_2 estimation, remain unvalidated. Transitioning to TRL 3–4 requires systematic testing across diverse skin tones, motion conditions, and hypoxia with reference measurements.

Testing was limited to four light-skinned volunteers (Fitzpatrick types I–III); the device has not been evaluated on darker skin tones (types IV–VI), leaving the core hypothesis of reducing melanin bias unproven. Although the design includes motion-reduction features (rigid-flex coupling, synchronized acquisition, accelerometer integration), their effectiveness has not been quantitatively verified through controlled motion experiments. Current firmware includes only basic heart rate estimation; validated SpO_2 and motion compensation algorithms require a large, diverse dataset not currently available.

Thermal management uses passive graphite sheet cooling with analytical estimates suggesting minimal LED wavelength drift (<0.2 nm). However, thermal characterization remains incomplete without simulations or experimental data on junction temperature or wavelength stability under continuous use.

To address these limitations, full clinical validation following FDA guidance [1] will include: arterial blood gas validation during controlled hypoxia; participant recruitment across all Fitzpatrick skin types (minimum $N = 10$ per group); motion artifact testing under standardized protocols; statistical analysis (Bland–Altman plots, ARMS error, subgroup bias/precision); and comparison with FDA-cleared oximeters. This study will assess which motion artifacts can be compensated, how performance varies by skin tone, and whether the multi-wavelength design reduces melanin-induced bias compared to standard two-wavelength systems.

Until validation is complete, these results establish a robust hardware platform demonstrating feasibility rather than evidence of clinical performance or measurement equity.

3.5. Potential applications and use cases

The engineering features demonstrated, ring form factor, rigid-flex anatomical coupling, and multi-wavelength optical acquisition, position the platform to address limitations where current devices fail due to motion artifacts, environmental challenges, and skin pigmentation bias.

The ring format enables unobtrusive monitoring during athletic activities where fingertip clips interfere with performance, including ventilatory and anaerobic threshold detection, altitude training, and high-intensity interval training. Stable mechanical coupling may reduce motion artifacts during running, cycling, or resistance training where conventional sensors lose signal [44]. Tactile-intelligence pulse oximetry has demonstrated up to 8-fold reduction in measurement error during exercise [19].

Patients with chronic cardiorespiratory diseases (post-COVID-19 sequelae, cystic fibrosis, pulmonary fibrosis, COPD, cardiac surgery recovery) may benefit from continuous monitoring during rehabilitation to prevent desaturation [4,45]. Wearable-assisted home cardiac rehabilitation programs have demonstrated improved peak VO_2 outcomes compared to center-based programs [46,47]. Recent validation studies of ring-form oximeters showed negligible bias across Black and non-Black participants during controlled hypoxia, suggesting proper sensor design can mitigate pigmentation effects [20].

High-risk occupational applications include firefighters facing high-G forces, extreme heat, and smoke exposure affecting signal quality through poor perfusion and sensor dislodgement [48,49], and fighter pilots experiencing high-G forces and fluctuating cabin pressure that challenge conventional oximetry [44]. The ring form factor remains functional beneath protective gloves [48].

Skin pigmentation bias represents a significant occupational safety concern, as systematic measurement errors could delay hypoxemia recognition in workers with darker skin during high-risk operations [4, 45]. The multi-wavelength design addresses melanin-induced optical

interference, ensuring equitable safety monitoring across diverse workforces.

Wireless design enables applications in sleep monitoring, post-discharge respiratory tracking, and telemedicine in remote or low-resource settings. Multi-wavelength capability is critical for telehealth serving diverse populations where clinicians cannot directly assess patient skin tone [8].

These use cases represent potential future applications requiring: validation against arterial blood gas analysis across the full SpO_2 range (70%–100%), quantitative motion artifact evaluation, assessment across all Fitzpatrick skin types (I-VI), regulatory clearance (FDA or CE marking), and validation within intended populations [50,51]. The platform establishes technical feasibility to pursue these validation steps, with emphasis on addressing documented skin pigmentation bias affecting conventional pulse oximetry [4,20]. Recent advances in multi-wavelength pulse oximetry and CO-oximetry platforms demonstrate clinical utility of enhanced spectral approaches for addressing pigmentation bias [8,52].

4. Conclusions

This work presents successful design, fabrication, and preliminary characterization of a wearable pulse oximeter platform addressing two critical limitations of conventional pulse oximetry: motion artifacts and skin pigmentation bias.

The innovation lies in three deliberate engineering strategies. First, rigid-flex PCB architecture enables a compact ring form factor ensuring mechanical stability and secure sensor-to-skin contact, reducing motion-induced signal distortions. Second, multi-wavelength optical design (610–940 nm) surpasses standard dual-wavelength models by generating high-fidelity photoplethysmographic signals across four channels, laying groundwork for algorithms that distinguish melanin absorption from hemoglobin dynamics, essential for equitable SpO_2 measurement. Third, heart-rate-synchronized acquisition represents early integration of intelligent sensing features for motion artifact suppression.

Preliminary testing on four volunteers (Fitzpatrick types I–III) confirmed reliable multi-wavelength PPG signal acquisition with improved signal quality at longer wavelengths (740–940 nm), validating the hardware platform's technical feasibility. However, critical limitations remain. The device has not been validated against arterial blood gas analysis across the full SpO_2 range (70%–100%), tested on darker skin tones (Fitzpatrick IV–VI), or evaluated under controlled motion conditions. SpO_2 estimation and motion compensation algorithms have not been developed, placing this work at Technology Readiness Level 2–3.

Future validation following FDA guidance will include: controlled hypoxia studies with arterial blood sampling across all Fitzpatrick skin types (minimum $N = 10$ per group); quantitative motion artifact assessment; statistical analysis (Bland–Altman plots, ARMS error, subgroup bias/precision); and comparison with FDA-cleared oximeters. Until this validation is complete, this platform establishes technical feasibility for future clinical studies aimed at developing next-generation point-of-care systems with improved accuracy and equity across diverse populations.

CRediT authorship contribution statement

Pilar Martín-Escudero: Writing – review & editing, Writing – original draft, Visualization, Validation, Supervision, Software, Resources, Project administration, Methodology, Investigation, Funding acquisition, Formal analysis, Conceptualization. **Ana M. Cabanas:** Writing – review & editing, Writing – original draft, Visualization, Validation, Supervision, Methodology, Formal analysis, Data curation, Conceptualization.

Funding

This work was supported by "Development of a portable pulse oximeter with Bluetooth output, for integration into the medical monitoring of post-COVID-19 patients, with in- and out-of-hospital respiratory rehabilitation" Project funded by Healthstart Plus (HSP-2; 2022).

Declaration of competing interest

The authors declare the following financial interests/personal relationships which may be considered as potential competing interests: Pilar Martin Escudero reports financial support was provided by Healthstart Plus (HSP-2 2022). Pilar Martin Escudero has patent Anillo oxímetro de pulso portátil con conexión bluetooth de baja energía para uso en condiciones de esfuerzo físico y para todo tipo de color de piel pending to Utility Model U202431452. If there are other authors, they declare that they have no known competing financial interests or personal relationships that could have appeared to influence the work reported in this paper.

Acknowledgments

The authors would like to thank Martín Lopo, Miguel; Vázquez Blanco, Antonio; Vicente Villaseca, César; and Marco Zamora, Jesús, for their valuable contributions as engineers to the development of this utility model. A.M.C. acknowledges support from the ANID - Millennium Science Initiative Program (iHealth) ICN2021_004, ANID Project SA77210039, and the Universidad de Tarapacá Mayor Project 4740-25.

Appendix A. Supplementary data

Supplementary material related to this article can be found online at https://doi.org/10.1016/j.sna.2025.117213.

Data availability

Data will be made available on request.

References

[1] U.S. Food and Drug Administration (FDA), Performance Evaluation of Pulse Oximeters Taking into Consideration Skin Pigmentation, Race and Ethnicity, U.S. Food and Drug Administration, 2024.
[2] Division of Industry and Consumer Education (DICE), Pulse Oximeter Accuracy and Limitations: FDA Safety Communication, United States Food and Drug Administration, FDA, 2021.
[3] Department of Health and Social Care, Equity in Medical Devices: Independent Review, Tech. Rep., Open Government Licence v3.0, 2024, pp. 1–127, URL www.gov.uk/dhsc. (Accessed December 2024).
[4] S. Singh, M. Bennett, C. Chen, et al., Impact of skin pigmentation on pulse oximetry SpO_2 and wearable pulse rate accuracy: A Meta-Analysis, J. Med. Internet Res. 26 (2024) e62769, http://dx.doi.org/10.2196/62769.
[5] B.W. Nelson, S. Singh, M. Bennett, et al., The impact of skin pigmentation on pulse oximetry SpO_2 and wearable pulse rate accuracy: A Meta-Analysis, 2024, http://dx.doi.org/10.21203/rs.3.rs-3882498/v1.
[6] N.C. Chunhu Shi, Mark Goodall, Jo Dumville, James Edward Hill , Gill Norman , Oliver Hamer , Andrew Clegg , Caroline Leigh Watkins , George Georgiou , Alexander Hodkinson , Catherine Elizabeth Lightbody , Paul Dark, C. Shi, M. Goodall, J. Dumville, J. Hill, G. Norman, O. Hamer, A. Clegg, C.L. Watkins, G. Georgiou, A. Hodkinson, C.E. Lightbody, P. Dark, N. Cullum, Article the effects of skin pigmentation on the accuracy of pulse oximetry in measuring oxygen saturation : a systematic review and meta-analysis the effects of skin pigmentation on the accuracy of pulse and meta-analysis, PLoS Med. (2022) http://dx.doi.org/10.1101/2022.02.16.22271062, URL https://www.medrxiv.org/content/early/2022/02/17/2022.02.16.22271062.
[7] Open Oximetry Project, Open oximetry, 2024, URL https://openoximetry.org/. (Accessed July 2025).
[8] T. Kong, A. Hedayatipour, Oximeter for all: An innovative look in inclusive physiological monitoring [Innovations Corner], IEEE Circuits Syst. Mag. 24 (3) (2024) 43–44, http://dx.doi.org/10.1109/MCAS.2024.3363608.

[9] R. Al-Halawani, P.H. Charlton, M. Qassem, et al., A review of the effect of skin pigmentation on pulse oximeter accuracy, Physiol. Meas. (2023) http://dx.doi.org/10.1088/1361-6579/acd51a.

[10] P.E. Bickler, J.R. Feiner, J.W. Severinghaus, Effects of skin pigmentation on pulse oximeter accuracy at low saturation, Anesthesiology 102 (4) (2005) 715–719, http://dx.doi.org/10.1097/00000542-200504000-00004.

[11] D. León-Valladares, L.A. Barrio-Mateu, N. Cortés-Carmona, G. Fuentes-Lizana, A.M. Cabanas, K. Latorre-Progulakis, M. Fuentes-Guajardo, P. Martín-Escudero, Determining factors of pulse oximetry accuracy: a literature review, Rev. Clín. Española (Engl. Ed.) 224 (5) (2024) 314–330, http://dx.doi.org/10.1016/j.rceng.2024.04.005, URL https://www.sciencedirect.com/science/article/pii/S2254887424000523.

[12] M. Bermond, H.J. Davies, E. Occhipinti, A. Nassibi, D.P. Mandic, Reducing racial bias in spo2estimation: The effects of skin pigmentation, in: Proceedings of the Annual International Conference of the IEEE Engineering in Medicine and Biology Society EMBS, IEEE, 2023, pp. 1–5, http://dx.doi.org/10.1109/EMBC40787.2023.10341069.

[13] R.M. Tobin, J.A. Pologe, P.B. Batchelder, A characterization of motion affecting pulse oximetry in 350 patients, Anesth. Analg. 94 (1 SUPPL.) (2002).

[14] P. Martín-Escudero, A.M. Cabanas, M.L. Dotor-Castilla, M. Galindo-Canales, F. Miguel-Tobal, C. Fernández-Pérez, M. Fuentes-Ferrer, R. Giannetti, Are activity Wrist-Worn devices accurate for determining heart rate during intense exercise? Bioengineering 10 (2) (2023) http://dx.doi.org/10.3390/bioengineering10020254, URL https://www.mdpi.com/2306-5354/10/2/254.

[15] P. Ghosal, S. Himavathi, E. Srinivasan, Improved method for motion artifact reduction from finger photoplethysmogram signal, Int. J. Intell. Syst. Appl. Eng. 11 (1) (2023) 190–194.

[16] M.A.H. S. Rea Mark, Bierman Andrew, LED spectra are the likely source of the systematic bias in pulse oximeter readings for individuals with darker skin pigmentation, Br. J. Anaesth. (2023).

[17] G. Leeb, I. Auchus, T. Law, P. Bickler, J. Feiner, S. Hashi, E. Monk, E. Igaga, M. Bernstein, Y.C. Chou, C. Hughes, D. Schornack, J. Lester, K.J. Moore, O. Okunlola, J. Fernandez, L. Shmuylovich, M. Lipnick, The performance of 11 fingertip pulse oximeters during hypoxemia in healthy human participants with varied, quantified skin pigment, EBioMedicine 102 (2024) 105051, http://dx.doi.org/10.1016/j.ebiom.2024.105051.

[18] C. Hughes, D. Chen, T. Law, P. Bickler, J. Feiner, L. Shmuylovich, E. Behnke, L. Ortiz, G. Leeb, I. Auchus, F. Negussie, R. Bisegerwa, R. Zamora, E. Igaga, K.J. Moore, O. Okunlola, E. Monk, J. Fernandez, O. Ehie, B. Wilks, K. Oyefeso, D. Schornack, C. Sendagire, M. Lipnick, Pulse oximeter performance and skin pigment: comparison of 34 oximeters using current and emerging regulatory frameworks, MedRxiv (2025) http://dx.doi.org/10.1101/2025.08.11.25332026, 2025-2008.

[19] S. Zhou, L. Zhao, J. Fang, T. Pan, Tactile intelligence enabled pulse oximeter for motion artifacts removal, in: 2025 IEEE International Conference on Flexible and Printable Sensors and Systems, FLEPS, 2025, pp. 1–4, URL https://api.semanticscholar.org/CorpusID:280538890.

[20] M.M.e. Cruz, C. Zhou, M.H. Kryger, et al., Validation of a smart ring oximeter in individuals with dark skin pigment, Mayo Clin. Proc.: Digit. Health 1 (3) (2023) 394–401, http://dx.doi.org/10.1016/j.mcpdig.2023.06.012.

[21] F. Salamone, M. Masullo, S. Sibilio, Wearable devices for environmental monitoring in the built environment: A systematic review, Sensors 21 (14) (2021) http://dx.doi.org/10.3390/s21144727, URL https://www.mdpi.com/1424-8220/21/14/4727.

[22] W.R. Thompson, Worldwide survey of fitness trends for 2023, ACSM's Health Fit. J. 27 (1) (2023) URL https://journals.lww.com/acsm-healthfitness/fulltext/2023/01000/worldwide_survey_of_fitness_trends_for_2023.6.aspx.

[23] V. Sharma, S.J. Barker, J. Novak, W.C. Wilson, Pulse oximetry performance in darkly pigmented skin: Methodological concerns, Anesth. Analg. 139 (6) (2024) e62–4, http://dx.doi.org/10.1213/ANE.0000000000007224.

[24] A.K. Maity, A. Veeraraghavan, A. Sabharwal, PPGMotion: Model-based detection of motion artifacts in photoplethysmography signals, Biomed. Signal Process. Control. 75 (2022) http://dx.doi.org/10.1016/j.bspc.2022.103632.

[25] RingConn, Why smart rings are the future of fitness, fashion, and wellness, 2024, URL https://ringconn.com/es/blogs/noticias/why-smart-rings-are-the-future-of-fitness-fashion-and-wellness. (Accessed 19 July 2025).

[26] S.L. Jacques, Optical properties of biological tissues: a review, Phys. Med. Biol. 58 (11) (2013) R37–R61.

[27] M.W. Sjoding, R.P. Dickson, T.J. Iwashyna, S.E. Gay, T.S. Valley, Racial bias in pulse oximetry measurement, New Engl. J. Med. 383 (25) (2020) 2477–2478, http://dx.doi.org/10.1056/NEJMc2029240, URL https://www.nejm.org/doi/full/10.1056/NEJMc2029240.

[28] A.M. Cabanas, P. Martín-Escudero, K.H. Shelley, Improving pulse oximetry accuracy in dark-skinned patients: technical aspects and current regulations, Br. J. Anaesth. 131 (4) (2023) 640–644, http://dx.doi.org/10.1016/j.bja.2023.07.005.

[29] O. Tsiakaka, B. Gosselin, S. Feruglio, Source-detector spectral pairing-related inaccuracies in pulse oximetry: Evaluation of the wavelength shift, Sensors 20 (11) (2020) 3302, http://dx.doi.org/10.3390/S20113302.

[30] D. Ray, T. Collins, S.I. Woolley, et al., A review of wearable Multi-wavelength photoplethysmography, IEEE Rev. Biomed. Eng. (2021) http://dx.doi.org/10.1109/RBME.2021.3121476.

[31] A. Bierman, K. Benner, M.S. Rea, Melanin bias in pulse oximetry explained by light source spectral bandwidth, Br. J. Anaesth. 132 (5) (2024) 957–963, http://dx.doi.org/10.1016/j.bja.2024.01.037.

[32] Panasonic Corporation, PGS (Pyrolytic Graphite Sheet) Thermal Management Solutions, Technical Datasheet, 2023.

[33] U. Food, D. Administration, Approach for Improving the Performance Evaluation of Pulse Oximeter Devices Taking Into Consideration Skin Pigmentation , Race and Ethnicity Discussion Paper and Request for Feedback Approach for Improving the Performance Evaluation of Pulse Oximeter Devi, Tech. Rep., FDA Safety Communication, 2023.

[34] P.M. Escudero, et al., Anillo oxímetro de pulso portátil con conexión bluetooth de baja energía para uso en condiciones de esfuerzo físico y para todo tipo de color de piel, 2024, National Utility Model U202431452. Filed: 29 July 2024. Granted: 8 April 2025. Oxifing Health Sport.

[35] L.S. Giannetti R, A. Sanchez Miralles, M. Dotor, P. Martín Escudero, F. Miguel Tobal, G.C. M, Sensor, device, system and method for determining intervals non invasive training for conducting an exercise, 2017, URL https://patents.google.com/patent/WO2017168029A1/es?inventor=DOTOR+CASTILLA2C&oq=DOTOR+CASTILLA2C, PCT/ES2017/070195 date:31 March 2017.

[36] L.S. Giannetti R, A. Sanchez Miralles, M. Dotor, P. Martín Escudero, F. Miguel Tobal, M. Galindo Canales, Sensor, device, system and method for determining non-invasive training intervals for conducting an exercise, 2025, Application admitted for processing, with copy forwarded to the International Bureau (WIPO). Filing date: July 24, 2025, PCT/ES2025/070460.

[37] C.Y. Chen, T.H. Yang, C.H. Hsu, K.H. Chen, Temperature-dependent optical properties of AlGaInP-based red and amber LEDs, IEEE Trans. Electron Devices 61 (4) (2014) 1226–1232, http://dx.doi.org/10.1109/TED.2014.2304886.

[38] J. Costa, H. Vieira, P. Louro, M. Vieira, Double junction photodiodes for multiwavelength photoplethysmography, in: Optical Sensing and Detection V, Vol. 10680, SPIE, 2018, pp. 542–548.

[39] J. De Kock, K. Reynolds, L. Tarassenko, J. Moyles, The effect of varying LED intensity on pulse oximeter accuracy, J. Med. Eng. Technol. 15 (3) (1991) 111–115.

[40] Panasonic Corporation, PGS Graphite Sheets Product Specifications, EYG-S Series, Technical Datasheet, Panasonic Corporation, 2023, Available: https://industrial.panasonic.com/ww/products/thermal-management.

[41] K.B. Kim, H.J. Baek, Photoplethysmography in wearable devices: A comprehensive review of technological advances, current challenges, and future directions, Electronics 12 (13) (2023) http://dx.doi.org/10.3390/electronics12132923, URL https://www.mdpi.com/2079-9292/12/13/2923.

[42] L. Finlayson, I. Barnard, L. McMillan, S. Ibbotson, C. Brown, E. Eadie, K. Wood, Depth penetration of light into skin as a function of wavelength from 200 nm - 1000 nm, Photochem. Photobiol. 98 (2021) http://dx.doi.org/10.1111/php.13550.

[43] E.J.A. Prada, On the development of an efficient, low-complexity and highly reproducible method for systolic peak detection, Biomed. Signal Process. Control. 70 (2021) 102606, http://dx.doi.org/10.1016/j.bspc.2021.102606.

[44] E.L. Hearn, J. Byford, C. Wolfe, et al., Measuring arterial oxygen saturation using wearable devices under varying conditions, Aerosp. Med. Hum. Perform. 94 (1) (2023) 1–8, http://dx.doi.org/10.3357/amhp.6078.2023.

[45] B.W. Nelson, S. Singh, M. Bennett, et al., The impact of skin pigmentation on pulse oximetry SpO_2 and wearable pulse rate accuracy: A Meta-Analysis, Res. Sq. (2024) http://dx.doi.org/10.21203/rs.3.rs-3882498/v1.

[46] L. Batalik, F. Dosbaba, M. Hartman, et al., Benefits and effectiveness of using a wearable device in a cardiac telerehabilitation program: systematic review, BMJ Open 11 (2) (2021) e044110, http://dx.doi.org/10.1136/bmjopen-2020-044110.

[47] J.C. Rawstorn, N. Gant, A. Direito, et al., Telehealth exercise-based cardiac rehabilitation: a systematic review and meta-analysis, Heart 102 (15) (2022) 1183–1192, http://dx.doi.org/10.1136/heartjnl-2015-308966.

[48] C. Barros, J.P.S. Cunha, et al., Physiological monitoring systems for fatigue detection within firefighters: A brief systematic review, in: Advances in Intelligent Systems and Computing, Vol. 1408, 2022, pp. 475–485, http://dx.doi.org/10.1007/978-3-031-12547-8_38.

[49] L. Chen, M. Wang, Y. Zhang, et al., Wearable sensor networks in emergency response: advances and challenges, IEEE Sens. J. 23 (12) (2023) 13245–13256, http://dx.doi.org/10.1109/JSEN.2023.3271234.

[50] FDA, Pulse Oximeters - Premarket Notification Submissions [510(k)s]: Guidance for Industry and Food and Drug Administration Staff, Tech. Rep., U.S. Food and Drug Administration, 2022.

[51] Medical electrical equipment - Part 2-61: Particular requirements for basic safety and essential performance of pulse oximeter equipment, 2021.

[52] J. Barker, R. Smith, M. Jones, et al., Utility of continuous pulse CO-oximetry for hemoglobin monitoring in pediatric patients with solid organ injuries at level 1 trauma centers: A pilot study, J. Trauma Acute Care Surg. (2023) http://dx.doi.org/10.1097/TA.0000000000003926.

Pilar Martín Escudero hold a Ph.D. in Medicine and Surgery (1997) and a specialization in Physical Education and Sports Medicine (1991), both from the Complutense University of Madrid (UCM), where I have worked since 1990. I have been a full professor with a permanent position at the School of Professional Medicine in Physical Education and Sports, Faculty of Medicine, since 2007. With over 25 years of professional and academic experience, I have dedicated my career to advancing sports medicine through teaching, research, and clinical practice.

My professional career includes extensive participation in major international sporting events as a physician for the Spanish Olympic team, serving at the 1992 Barcelona, 2012 London, 2020 Tokyo Olympic Games and 2024 Paris, as well as the 2013 and 2017 Deaflympics. I have carried out more than 200 doping controls for various sports federations and contributed to anti-doping education and policy. My doctoral research focused on the application of oximetry in maximal exercise testing, establishing a link between oxygen saturation and athletic performance.

Throughout my academic career, I have taught over 400 sports medicine physicians, participated in more than 25 research projects, and supervised six doctoral theses. My research has led to four patents in biomedical engineering applied to sports and several national and international awards, including the National Prize for Sports Medicine Research and the UCM-Santander Innovation Award. I have authored numerous publications, delivered over 50 lectures worldwide, and currently serve as Director of the School of Physical Education and Sports Medicine (since February 2025), member of the Spanish Olympic Committee Medical Commission, and CEO of Oxifing Health Sport, a company developing wearable health technology for athletes.

Ana María Cabanas Plana holds a Ph.D. in Physics from the Universidad de Tarapacá, Chile, and a Licentiate degree in Physics from the Universidad Complutense de Madrid, Spain. She currently serves as an academic at the Department of Physics, Universidad de Tarapacá, where her research bridges theoretical physics and applied biomedical technologies. Her recent work focuses on signal processing and machine learning applications in pulse oximetry, with particular interest in algorithmic bias, physiological variability in athletes, and regulatory aspects of AI-based medical devices. Dr. Cabanas has authored multiple peer-reviewed articles in high-impact journals such as British Journal of Anaesthesia, Bioengineering, and Biosensors, and often collaborates on interdisciplinary studies combining physics, physiology, and AI. Her broader scientific interests include nonlinear dynamics, entropy analysis, and health technology evaluation.